| | |
|---|---|
| Title | High-Q micromechanical resonators for mass sensing in dissipative media |
| Author(s) | Tappura, Kirsi; Pekko, Panu; Seppä, Heikki |
| Citation | Journal of Micromechanics and Microengineering vol. 21(2011):6, s. 065002 |
| Date | 2011 |
| URL | http://dx.doi.org/10.1088/0960-1317/21/6/065002 |
| Rights | Copyright © (2011) IOPscience. Reprinted from Journal of Micromechanics and Microengineering. This article may be downloaded for personal use only |

*Accepted for publication in Journal of Micromechanics and Microengineering 2011*

# High-Q micromechanical resonators for mass sensing in dissipative media

**Kirsi Tappura[1,*], Panu Pekko[2], and Heikki Seppä[2]**

[1]VTT Technical Research Centre of Finland, P.O. Box 1300, FI-33101 Tampere, Finland

[2]VTT Technical Research Centre of Finland, P.O. Box 1000, FI-02044 VTT, Finland

**E-mail:** kirsi.tappura@vtt.fi

**Abstract.** Single crystal silicon based micromechanical resonators are developed for mass sensing in dissipative media. The design aspects and preliminary characterization of the resonators are presented. For the suggested designs, quality factors of about 20000 are typically measured in air at atmospheric pressure and 1000-2000 in contact with liquid. The performance is based on a wine-glass type lateral bulk acoustic mode excited in a rectangle resonator plate. The mode essentially eliminates the radiation of acoustic energy into the sample media leaving viscous drag as the dominant fluid-based dissipation mechanisms in the system. For a mass loading distributed over the central areas of the resonator a sensitivity of 27 ppm/ng is measured exhibiting good agreement with the results of the finite element method based simulations. It is also shown that the mass sensitivity can be somewhat enhanced, not only by the proper distribution of the loaded mass, but also by introducing shallow barrier structures on the resonator.

PACS codes: 85.85.+j, 46.40.Ff, 43.20.Tb, 43.40.Dx, 07.07.Df, 87.85.fk, 07.05.Tp

Key words: Mass sensor; MEMS resonator; Quality factor; Lateral bulk acoustic wave; Wine-glass mode.

## 1. Introduction

There is a growing demand for small, cost efficient array type sensors that can perform analysis of different marker molecules or substances in various environments. A well known approach is to use acoustic resonators as mass sensors where the shift of the resonant frequency corresponds to the mass adsorbed onto the resonator [1]. In addition to the conventional piezoelectric, quartz crystal based, thickness shear mode sensors (so called quartz crystal microbalance, QCM, sensors) , different piezo actuated thin film bulk acoustic resonators (FBAR) have been demonstrated for gravimetric sensing especially for applications requiring higher level of integration. When designed to vibrate in a shear mode, the FBAR sensors can operate with moderate quality factors (Q factors, Q values) in liquid (150 - 200) as well as in air (300 - 400) [2-3]. The micro/nanomechanical mass sensors reported are typically based on cantilever structures [4-5]. Such flexural mode resonators, however, exhibit limited quality factors already in air and experience severe damping in liquid resulting to very low Q values, typically of the order of 1 in water [6]. The problem is usually circumvented by using a, so called, static or bending mode [7], which, however, looses the benefits of the resonance phenomenon and – with the coatings required – tends to complicate the interpretation of the results [8]. A different approach has also been introduced: viscous loss could be nearly eliminated by placing the fluid inside of a hollow resonant cantilever surrounded by vacuum [9].

Impressive quality factors are relatively easy to obtain for mechanical resonators at reduced pressures or in vacuum [10-11]. When small masses need to be measured at atmospheric pressure and especially in liquid, special attention needs to be paid to the resonator design for minimizing the fluid-based energy dissipations, such as to minimize the radiation of acoustic energy into the surrounding medium., to avoid squeezed film damping in small gaps and, finally, to sustain the vibrations despite the inevitable viscous forces. Related to this and compared to the mass sensors mentioned above, single crystal silicon (SC-Si) based lateral bulk acoustics wave (BAW) resonators have distinct benefits: 1) Microelectromechanical systems (MEMS) based on SC-Si have excellent mechanical properties with intrinsic capabilities for integration and size scaling. 2) BAW resonators have significantly higher energy storage capacity compared, for example, to flexural mode devices. 3) The maximum power with which a BAW device can be driven is also orders of magnitude higher than that for a flexural mode resonator [10]. 4) Finally, the out-of-plane vibrations can efficiently be minimized with lateral BAWs. All these features have direct influence also to the fundamental limit of mass detection imposed by thermomechanical noise [12]: The higher the resonant frequency and the Q value and the lower the effective mass of the resonator, the better the resolution. In addition, the higher the mechanical energy stored by the resonator, i.e. the higher the displacement amplitude and the vibrating volume, the better the Q value and the resolution.

Following the line of thought presented above we have previously described beneficial lateral BAW based resonant systems for mass sensing applications in dissipative media [13]. Recently, mass sensing with lateral BAW devices, in vacuum and in air, has also been reported by other groups [14-15].

The primary goal of this work was to design generic, SC-Si MEMS based, resonant mass sensors that can be used both in gas at atmospheric pressures and in contact with liquid with high Q values. No ultimate mass resolution or sensitivity was aimed at as such but the goal was to demonstrate the potential of the proposed structures as mass sensors. In this paper, the design considerations with theoretical calculations, as well as computational and experimental results, are reported for one of the most promising structures.

## 2. Theoretical and computational resonator design

A high-Q, low-noise square extensional (SE) mode resonator was a starting point of the development work [16]. After some theoretical investigations, rectangular SC-Si resonator plates operating in a wine-glass [10, 17] type mode (called here as an RWG mode) were selected for

more intensive studies due to their benefits for operating in contact with liquid. Figure 1(a) illustrates the RWG mode by displaying the relative displacements of various locations on the plate obtained from the finite element method (FEM) simulations [18] where the surface of the plate is oriented along the {100} and the sides along the {110} crystal planes. The elastic constants of ref. [19] and the density ($\rho_{Si}$) of 2329 kg/m$^3$ are applied for SC-Si in the simulations. T-shaped corner anchors are used to support the plate. Shallow basin/barrier structures (4.6 μm in depth) are also shown as etched on the 25 μm thick plate [see figure 1(b)] to enable the confinement of liquid to the central area where the maximal lateral displacements occur [figure 1(a)]. In order not to degrade the electromechanical coupling non-etched slices are also left close to the electrodes. The shallow barrier structures, designed to locate at the nodal positions or close to the areas of minimal displacement where possible, do not degrade the acoustic (RWG) mode according to the simulations.

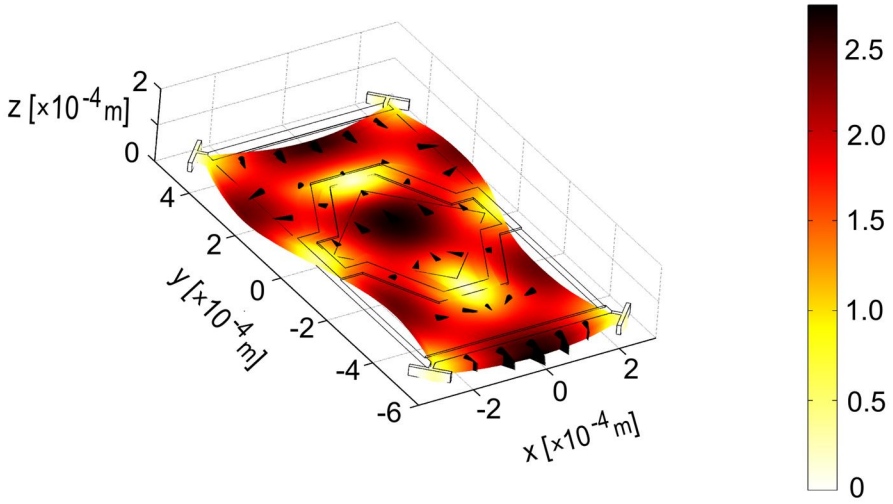


(a)

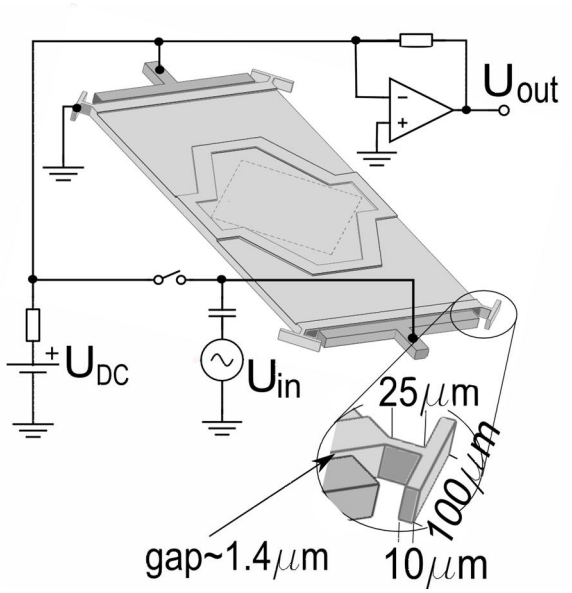


(b)

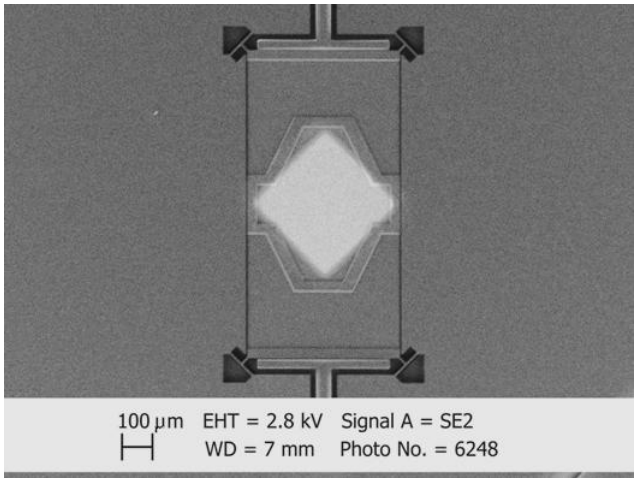


(c)

**Figure 1.** (a) The RWG mode of a rectangle resonator illustrated by the relative displacements of various locations on the plate (indicated by color coding, black arrows and the exaggerated deformation of the shape). The length (990 µm) to width (495 µm) ratio of the plate is 2. (b) A schematic illustration of the resonator and its measurement setup. The square sketched in the middle of the plate shows the initial gold area and the loaded mass used in the simulations of figure 3. (c) A SEM micrograph of the resonator.

The RWG mode is a Lamé [17] type mode where the corner points are fixed, edges bend in anti-phase and the volume is conserved. Such an isochoric mode exhibits about three orders of magnitude smaller energy losses due to thermoelastic damping than e.g. a SE or a non-isochoric "Lamé" type mode [20] and provides optimal nodal positions for the stem connections at the corners to minimize the anchoring losses. It can also be shown that for the crystal orientations and dimensional relations used the Poisson contractions in the off-plane (z) direction vanish for an ideal square plate, and thus, also for an ideal rectangle plate that can be considered to consist of such squares stacked in-plane [17]. Due to the negligible off-plane displacements the radiation of acoustic energy into the media in contact with the top (x-y) surface of the plate is minimal. This is essential when operating in contact with e.g. water or other media having their acoustic impedance close to that of silicon.

The RWG mode propagating in a rectangular plate can be approximated by two sinusoidal acoustic waves with the displacements in the x and y directions described as $u_x = +A\cos(\pi y/L)\cos(\pi x/L)$ and $u_y = -A\sin(\pi x/L)\sin(\pi y/L)$, respectively, while $u_z = 0$. Here $A$ is the amplitude and $L$ the period of the acoustic wave in the x and y directions [see figure 1(a)]. To support the desired mode approximated by displacement functions $u_x$ and $u_y$, the width of the resonator was set to $L$, the length to $2L$ and the range of x from –L/2 to L/2 and y from –L to L with respect to the plate dimensions as shown in the figure. Further, by generating a counterclockwise rotation of 45° around z axis in the xy-plane for $x$, $y$, $u_x$ and $u_y$, we get $x' = 1/\sqrt{2}(x-y)$, $y' = 1/\sqrt{2}(x+y)$, $u_{x'} = \frac{1}{\sqrt{2}}\cos\left[\frac{\sqrt{2}\pi x'}{L}\right]$ and $u_{y'} = \frac{1}{\sqrt{2}}\cos\left[\frac{\sqrt{2}\pi y'}{L}\right]$. These formulas show that the wave can be considered as the superposition of two shear waves propagating along the diagonals of an $L\times L$ square. From the displacement functions we can calculate an approximate value for the effective mass: $m_{eff} = \rho h L^2 = ½\ m_{plate}$, where $h$ is the thickness and $m_{plate}$ the mass of the $L\times 2L$ rectangle plate.

The resonant frequency, $f_r$, of a rectangle SC-Si resonator with the sides of length $L$ and $2L$ (or a square resonator of side length $L$ [17]) aligned along the {110} crystal planes vibrating in the RWG mode can be approximated by

$$f_r = \frac{1}{\sqrt{2}L}\sqrt{\frac{G}{\rho_{Si}}} \quad (1)$$

where $G$ is the corresponding shear modulus (79.6 GPa) [19]. This gives $f_r \approx 8.35$ MHz for a resonator of size 495 μm by 990 μm.

In general, mass loading on a resonator causes a shift in the resonant frequency ($\Delta f$) that can be approximated by

$$\frac{\Delta f}{f_r} = -\frac{1}{2}\frac{\Delta m}{m_{eff}}, \quad (2)$$

assuming the stiffness of the resonator does not change when mass $\Delta m$ is added and $\Delta m << m_{eff}$.

## 3. Experimental

### *3.1 Device fabrication*

Highly boron doped (resistivity ~10-20 mOhm·cm) <100> oriented 150 mm silicon-on-insulator (SOI) wafers with a 1 μm thick buried oxide layer, a 25 μm thick SOI device layer and pre-etched cavities [21] (so called CSOI wafers [22]) were applied in the resonator fabrication. The main steps of the fabrication process are shown in figure 2.

4.4.-4.8 μm deep basin structures were etched on the rectangle resonator plates supported at the corners with T-shaped anchors, as show in figure 1. The width of the actuation/release gaps around the resonators was 1.3-1.5 μm. A thin gold layer of size 293 by 293 μm$^2$ with a TiW adhesion layer was deposited in the middle of the resonator plate with the nominal thicknesses of the Au and TiW layers 20 nm and 10 nm, respectively. The position of the square is shown in figure 1(c). The purpose of the gold layer, although not utilized in this work, was to enable the immobilization of molecule specific layers onto the gold surface via thiol chemistry. All the surfaces, except the gold areas, were covered with a 36-41 nm thick hydrophobic $C_4F_8$ plasmapolymer layer to improve the confinement of liquid on the resonator and to prevent it from entering in the actuation/release gaps or under the plates.

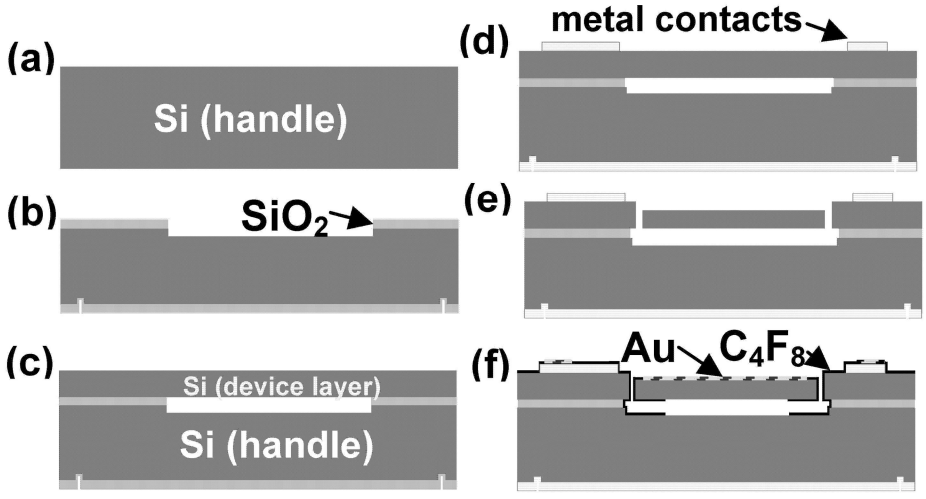


**Figure 2.** Fabrication process flow to obtain free standing rectangular resonators supported at the corner points with T-shaped anchors (see figure 1). The process comprises of the following steps: a) a double side polished (DSP) wafer as a starting material, b) cavity etching with deep reactive-ion etching (DRIE), c) wafer bonding and SOI layer thinning, d) patterning of metal contacts, e) release etching with DRIE, f) deposition of hydrophobic $C_4F_8$ plasmapolymer, removing it from the central areas of the plates by oxygen plasma etching through a shadow mask, and finally, deposition of gold through the same shadow mask.

*3.2. Measurement setup*

The transmission characteristics of the resonators ($S_{21}$) were measured using a network analyzer (Agilent E5070B) with a transimpedance preamplifier [figure 1(b)]. The vibrating plate, as well as the handle wafer and the device layer, excluding the electrodes and their contacts, were grounded. The drive signal was applied to the electrode at one end of the plate for capacitive actuation and the opposite actuation gap was used for readout. Clearly, the setup does not provide the most efficient electromechanical coupling, but compromises were necessary to enable safe introduction of liquid on the central area of the resonator far enough from the electrodes.

In capacitive coupling the force is proportional to the voltage squared of the drive signal. In the case of DC biased drive, where the drive signal $U = U_{DC} + \hat{u}_{ac}cos(\omega t)$ consists of the DC bias, $U_{DC}$, and an AC signal of amplitude $u_{ac}$, [i.e. the switch in figure 1(b) is closed], the force to the resonator is generated at the drive frequency, while in AC biased drive the drive/bias signal is simply $U = \hat{u}_{AC}\,cos(\omega t)$ [the switch in figure 1(b) open] resulting to a force of the form

$$F_{ac} \approx -\frac{\hat{u}_{AC}^2 C_0}{4d}\left[1+\cos(2\omega t)\right], \qquad (3)$$

where $\hat{u}_{AC}$ is the amplitude of the AC drive voltage [$U_{in}$ in figure 1(b)], $\omega$ the angular frequency, $d$ the gap size and $C_0$ the capacitance with a zero displacement. Thus, to excite the resonator at $f_r$, an input signal at $f_r/2$ is required. To gain equivalent forces with the DC and AC biased drives, i.e. $F_{ac} = F_{dc}$, the following equation needs to be satisfied: $\hat{u}_{AC} = \sqrt{4U_{DC}\hat{u}_{ac}}$. For example, $\hat{u}_{AC}$ = 20 V in an AC drive generates a force equal to that generated by a DC biased drive with $U_{DC}$ = 70 and $\hat{u}_{ac}$ = 1.5 V.

In the measurements an AC biased drive ($\hat{u}_{AC}$ = 20 V) was used with a DC biased ($U_{DC}$ = 70 V) readout. Here the main advantage of the AC bias comes from the fact that when the drive signal is at a different frequency from that of the readout so are also the unwanted currents due to parasitic capacitances.

## 4. Results and discussion

FEM simulations on mass loading [18] were performed for various resonators. In figure 3 the change in the resonant frequency is depicted as a function of the mass added on the center of the plate. The RWG mode resonators were simulated as described in section 2. The location of the added mass is shown in figure 1(b) as a square of size 293 μm by 293 μm sketched in the central basin. In the simulations the thickness of the layer of the added mass was varied between 5 and ~200 nm while keeping the density (1000 kg/m$^3$) and stiffness (1 GPa) constant. The stiffness of the layer was set small compared to that of silicon [19] in order not to increase the effective stiffness of the structure but to simulate the mass sensing properties.

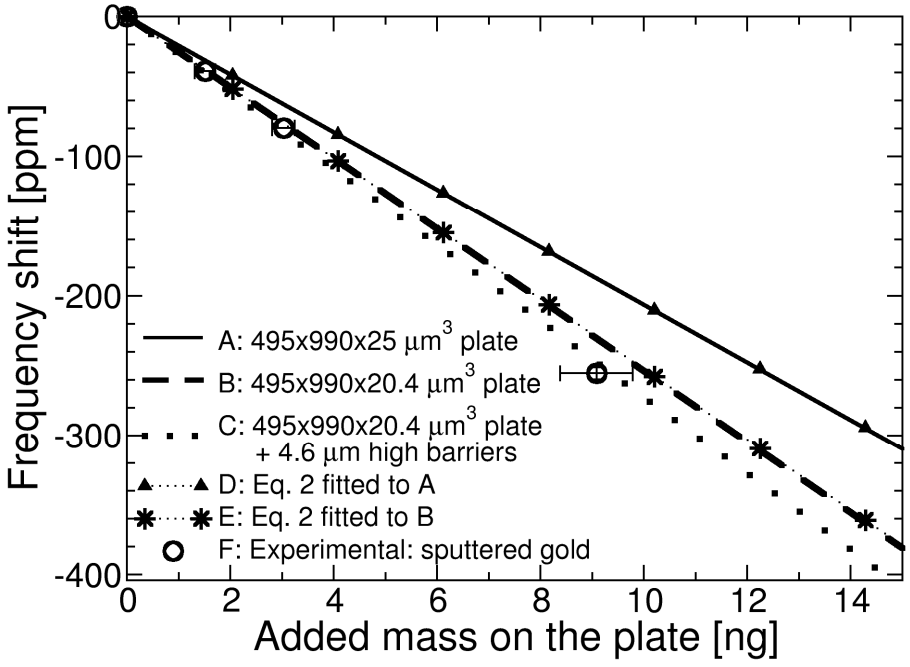


**Figure 3.** Relative frequency shifts for various resonators as a function of mass added on the center of the vibrating plate obtained by FEM simulations (curves A-C). The area of the added thin layer is 0.086 mm$^2$ and its location is shown in figure 1(b) as the square sketched on the basin. The thickness of the simulated layer was varied between 5 and ~200 nm while keeping the density (1000 kg/m$^3$) and stiffness (1 GPa) constant. Open circles (F) indicate the experimental data for the added mass of 0, 0.5, 1 and 3 nm thick gold layers sputtered on the central area of ~0.157 mm$^2$.

It can be seen that the thicker the plate the smaller the response, as expected from equation 2. In addition, the designed basin/barrier structures on the plate appear to steepen the slope, or increase the mass sensitivity, when compared to a plate of equal thickness but without the barriers (curve B vs. curve C in figure 3). This seems to be contrary to the fact that the barriers increase the total mass of the resonator. Nevertheless, the additional mass of the barriers should have relatively small influence on the effective mass of the resonator due to the fact that the barriers are mostly located at the points of minimal displacement. More detailed comparisons of the simulated displacement distributions of the RWG mode on different resonator plates revealed, however, that for the resonators with the barrier structures the relative displacements are about 10-15 % higher at the centre of the plate than at the four displacement maxima on the long edges of the same plate [see figure1(a)], while for a plate without the barriers all the maxima, both at the centre and near the edges, show very similar displacements. Thus, the structures etched on the resonator appear to somewhat enhance or concentrate the acoustic mode, or the relative amplitude of the lateral displacements, and therefore, increase the mass sensitivity at the central area of the plate. The results are in accordance with the previous observations that the mass sensitivity distribution on the surface of a quartz crystal resonator closely follows the vibration amplitude distribution of the resonator [23].

As shown above in Section 2, theoretically $m_{eff} \approx \frac{1}{2}\, m_{plate}$ for the RWG mode of a rectangle resonator. However, application of equation 2 is not straight forward for the data shown in figure 3, because the layer of added mass is distributed over a relatively large area around the centre of the resonator covering not only the points of maximal displacement. Equation 2 can be fitted to the simulated curves (D fitted to A and E to B in figure 3) by setting $m_{eff} \approx 0.85 m_{plate}$. This means that the apparent "effective mass" of the resonator seems higher for the distributed mass loading in question than what equation 2 predicts for a localized added mass at the point of maximal displacement, as expected in the effective mass approximation. Cagliani et al. have previously reported on related observations for a bulk disk resonator under different mass loadings [24]. The mass sensitivities obtained from the slopes of curves A, B and C are 21, 25, and 27 ppm/ng,

respectively. The corresponding sensitivities with respect to the surface mass densities are 18, 22 and 23 ppm·cm$^2$/μg when calculated for the area of the added mass (293×293 μm$^2$) and 103, 123 and 132 ppm·cm$^2$/μg for the total area of the resonator.

Experimental data obtained by sputtering thin gold layers through a shadow mask on the central area of a resonator is also shown in figure 3. The thicknesses of the layers were 0.5, 1 and 3 nm and the area ~0.157 mm$^2$. The data agrees well with the FEM simulations (curve D in figure 3) suggesting that no significant change in the effective stiffness of the structure occurs with such thin gold layers. On the other hand, the films were deposited mainly on the areas of maximal displacement and minimal strain, and therefore, the response to the possible changes in the strain is not expected to be very significant in any case. Figure 4 depicts the transmission responses ($S_{21}$) measured in air for the selected thicknesses of gold sputtered on the RWG mode resonator.

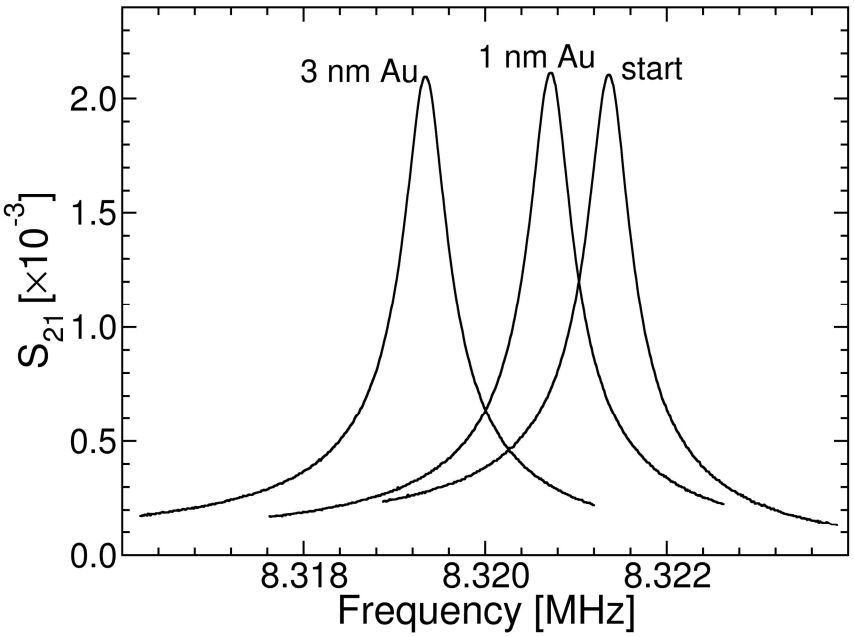


**Figure 4.** Transmission responses of an RWG mode resonator of figure 1 for different thicknesses of gold on the plate measured in air at atmospheric pressure. The added gold covers an area of ~0.157 mm$^2$ at the centre of the resonator.

In figure 5 the $S_{21}$ response is shown for a resonator of figure 1 in air and with the central basin filled with water. A plastic cover with shallow sample cuvettes around the resonators and holes for water injection was used in the measurements to control the liquid and to prevent the evaporation. Similar to the data shown in figure 5, the Q values, based on the measured $S_{21}$ resonance frequency and 3dB bandwidth are typically ~20000 in air at atmospheric pressure and vary in the range of 1000-2000 in contact with liquid i.e. with the basin of the resonator plate filled with water or a liquid of similar viscous properties. The values were determined for more than 30 samples. The measured Q values in air are about a factor of two higher than those typically reported for MEMS resonators at corresponding pressures [1, 7]. The measured Q values, both in air and in contact with liquid, are also order(s) of magnitude higher than the corresponding values reported for FBAR or cantilever resonators and similar to those of QCM [1-4, 25].

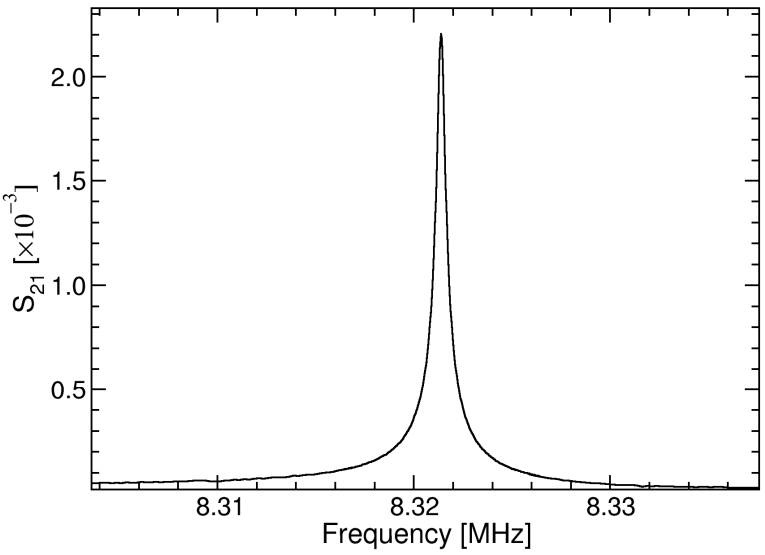


(a)

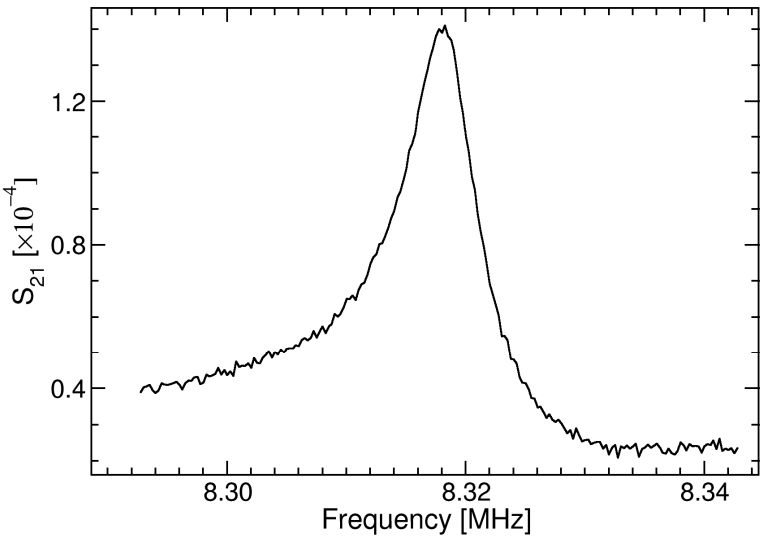


(b)

**Figure 5.** Transmission responses of an RWG mode resonator measured (a) in air at atmospheric pressure (Q = 19800) and (b) in contact with liquid (Q = 1740), i.e. with the central basin (see figure 1) filled with water.

As described in Section 2 damping caused by the radiation of acoustic energy into the fluid should be minimal with the designed resonators. Further, since the squeeze film damping in the actuation/release gaps is similar – and relatively small according to the measured Q in air – both for the measurements in air and in contact with liquid, viscous drag is expected to be the dominant cause of the energy dissipations with liquid. To estimate the influence of viscous damping on the Q value, the solution of the Navier-Stokes equation for an incompressible fluid on a resonator vibrating parallel to its plane surface is used. Following the procedure of Vignola et al. [26], the vibrating surface in contact with liquid, $A$, is divided into elements $A_i$, small enough that the phase

and the vibration velocity $v_i = v_{0i}e^{-j\omega t}$, where $j = (-1)^{1/2}$, can be considered approximately uniform over $A_i$. For such a system [27], the viscous force on $A_i$ can be expressed as

$$F_{vis,i} = \sqrt{\tfrac{1}{2}\omega\eta\rho_{fluid}}\,(j-1)v_i \qquad (4)$$

where $\eta$ and $\rho_{fluid}$ are the viscosity and density of the fluid and $\omega = 2\pi f_r$ the angular resonant frequency. The energy dissipated per unit time on $A_i$ can then be written

$$E_{vis,i} = \tfrac{1}{2}v_{0i}^{\,2}\sqrt{\tfrac{1}{2}\omega\eta\rho_{fluid}}\,A_i\,. \qquad (5)$$

The quality factor is defined as $2\pi$ times the ratio of the total energy stored in the resonator to the energy dissipated per cycle. When the stored energy is expressed as the peak kinetic energy $E_{kin} = \tfrac{1}{2}\, m v_{0i}^{\,2}$, the quality factor limited by viscous damping ($Q_{vis}$) can be written for the rectangle resonator as

$$Q_{vis} = \rho_{Si} h \frac{2L^2}{A}\sqrt{\frac{2\omega}{\eta\rho_{fluid}}}\,, \qquad (6)$$

where $h$ is the thickness of the resonator plate.

Table 1 lists the $Q_{vis}$ values calculated for different water contact areas on the resonator. It can be seen that the measured Q factors for the resonators in contact with water (e.g. $Q \approx 1740$ in figure 5) are in good agreement with the calculated $Q_{vis}$ values suggesting that viscous damping is the dominant dissipation mechanism in this case. The variations in the measured Q values (1000-2000) with the basin of the resonator plate is filled with water can be explained by the changes in the contact area of the liquid to the resonator: According to the calculations, for example, $Q_{vis}$ is 1900 when the contact area covers the bottom of the central basin, and decreases to 1270, if the contact area is increased by the area of the central barriers. Further, it is interesting to see that, according to Table 1, the Q value is expected to settle to about 500, if the resonator were fully covered by a water droplet.

**Table 1.** Calculated $Q_{vis}$ values for different areas of water on a resonator of size 495 μm by 990 μm vibrating parallel to its plane surface.

| Description of the water contact area on the resonator with respect to the features shown in figure 1 | Water contact area, $A$ ($m^2$) | Ratio of $A$ to the area of the resonator, $A/(2L^2)$ | Calculated $Q_{vis}$ |
|---|---|---|---|
| Square in the central basin | $8.6113\times10^{-8}$ | 0.18 | 2940 |
| Bottom of the central basin | $1.3349\times10^{-7}$ | 0.25 | 1 900 |
| Bottom and the area of the barriers of the central basin | $1.9881\times10^{-7}$ | 0.41 | 1 270 |
| Top area of a L×2L plate | $4.9005\times10^{-7}$ | 1 | 520 |
| No water, only air at NTP conditions on a L×2L plate | 0 | 0 | 104 360 |

In order to get an approximation of the resolution of the resonator as a mass sensor under the unoptimized measurement conditions used, sequential measurements of $S_{21}$ were performed in air and the standard deviation of $f_r$ was calculated from the data to estimate the frequency noise. When an estimated frequency noise of 0.1 ppm and the mass sensitivity of 27 ppm/ng obtained for the sputtered gold are applied, a mass resolution of ~ 3.7 pg can be deduced for the experiments presented above. As discussed with the results of figure 3, it should be noticed, however, that the mass sensitivity and, thus, the resolution also depend on the distribution of the added mass on the resonator.

## 5. Conclusions

The main design aspects and preliminary characterization of a rectangle bulk acoustic resonator as a mass sensor was presented. High quality factors both in air and in contact with liquid were demonstrated for the RWG mode resonant MEMS sensors and the origin of the results were discussed. A new way to provide some enhancement in mass sensitivity was also proposed. The results presented suggest that single crystal silicon based MEMS resonators can still open up new design options for sensitive mass detection of both liquid and gaseous samples. The potential of the proposed sensors is further emphasized by the fact that the silicon based microsystems technologies provide intrinsic capabilities for the fabrication of multi-sensor arrays as well as for integration.

## Acknowledgments

This work was supported in part by the Finnish Funding Agency for Technology and Innovation (grant 40405/05), Okmetic (incl. CSOI wafers), VTI Technologies, Environics, BioNavis and VTT. The authors wish to thank Mr. Timo Flyktman for the excellent technical work with the measurements and Mr. Jussi Tuppurainen for writing the first version of the Labview measurement software

## References

[1] Lucklum R and Hauptmann P 2006 Acoustic microsensors—the challenge behind microgravimetry *Anal. Bioanal. Chem.* **384** 667-82, and references therein.
[2] Wingqvist G, Bjurström J, Liljeholm L, Yantchev V, Katardjiev I 2007 Shear mode AlN thin film electro-acoustic resonant sensor operation in viscous media *Sens. Actuators B* **123** 466–73.
[3] Link M, Weber J, Schreiter M, Wersing W, Elmazria O, Alnot P 2007 Sensing characteristics of high-frequency shear mode resonators in glycerol solutions *Sens. Actuators B* **121** (2007) 372–8.
[4] Langa H P, Hegner M and Gerbera C 2005 Cantilever array sensors *Materials Today* **8** 30-6.
[5] DeMartini B E, Rhoads J F, Zielke M A, Owen K G, Shaw S W, Turner K L 2008 A single input-single output coupled microresonator array for the detection and identification of multiple analytes *Appl. Phys. Lett.* **93** 054102.
[6] Humphris A. D. L., Tamayo J., and Miles M. J. 2000 Active Quality Factor Control in Liquids for Force Spectroscopy *Langmuir* **16** 7891-4.
[7] Raiteri R, Nelles G, Butt H J, Knoll W and Skladal P 1999 Sensing of biological substances based on the bending of microfabricated cantilevers *Sens. Actuators B* **61**, 213-17.
[8] Dufoura I, Josseb F, Heinrichb S, Lucata C, Ayelaa C, Ménila F and Brandc O 2010 Unconventional uses of cantilevers for chemical sensing in gas and liquid environments *Procedia Engineering* **5** 1021–6.
[9] Burg T P, Godin M, Knudsen S M, Shen W, Carlson G, Foster J S, Babcock K, Manalis S R 2007 Weighing of biomolecules, single cells and single nanoparticles in fluid *Nature* **446** 1066-9.
[10] Lee J E-Y, Yan J, and Seshia A A 2009 Low loss HF band SOI wine glass bulk mode capacitive square-plate resonator *J. Micromech. Microeng.* **19** 074003.
[11] Khine L and Palaniapan M 2009 High-Q bulk-mode SOI square resonators with straight-beam anchors *J. Micromech. Microeng.* **19** 015017,
[12] Ekinci K L, Yang Y T and Roukes M L 2004 Ultimate limits to inertial mass sensing based upon nanoelectromechanical systems *J. Appl. Phys.* **95** 2682-9.
[13] Seppä H, Tappura K, Tuppurainen J, Mattila T, Alastalo A, Helle H, and Oja A Micromechanical sensor, sensor array and method, 2007. Pat. WO2007006843 A1 , priority FI2005739A.
[14] Agache V, Cochet M, Blanc R, Baleras F and Caillat P 2009 High Q factor plate resonators for ultrasensitive mass sensing applications *IEEE Transducers 2009*, Denver, CO, USA, June 21-25, 2009, pp. 1630-3.
[15] Lee J E-Y, Bahreyni B, Zhu, Y and Seshia A A 2007 Ultrasensitive mass balance based on a bulk acoustic mode single-crystal silicon resonator *Appl. Phys. Lett.* **91** 234103.
[16] Kaajakari V, Mattila T, Oja A, Kiihamäki J and Seppä H 2004 Square-Extensional Mode Single-Crystal Silicon Micromechanical Resonator for Low-Phase-Noise Oscillator Applications *IEEE Electron Device Lett.* **25** 173-5.
[17] Bourgeois C, Steinstand E, Blanc N, and de Rooij N F 1997 Design of resonators for the determination of the temperature coefficients of elastic constants of monocrystalline silicon, *Proceedings of the 1997 IEEE International Frequency Control Symposium* pp. 791–9.
[18] COMSOL Multiphysics 3.5a, Comsol AB: Stockholm, Sweden, www.comsol.com.
[19] McSkimin H J, Bond W L, Buehler E and Teal G K 1951 Measurement of the elastic constants of silicon single crystals and their thermal coefficients *Phys. Rev.* **83** 1080.
[20] Chandorkar S A, Agarwal M, Melamud R, Candler R N, Goodson K E and T. W. Kenny, 2008 Limits of quality factor in bulk-mode micromechanical resonators *IEEE 21st International Conference on Microelectromechanical Systems, IEEE MEMS* pp. 74-77.
[21] Luoto H, Henttinen K, Suni T, Dekker J, Mäkinen J, Torkkeli A 2007 MEMS on cavity-SOI wafers *Solid-State Electronics* **51** 328–332.
[22] The CSOI wafers are nowadays available from Okmetic Oyj.
[23] Mecea V.M. 2005 From quartz crystal microbalance to fundamental principles of mass measurements *Analytical Letters* **38** 753–767.

[24] Cagliani A and Davis Z J 2009 Bulk disk resonator based ultrasensitive mass sensor *Proceedings of the IEEE SENSORS 2009 Conference* Canterbury, New Zealand pp. 1317-20.
[25] Rodríguez-Pardo L, Fariña Rodríguez J, Gabrielli C, Perrot H and Brendel R 2005 Sensitivity, Noise, and Resolution in QCM Sensors in Liquid Media *IEEE Sensors Journal* **5** 1251-7.
[26] Vignola J F, Judge J A, Jarzynski J, Zalalutdinov M, Houston B H., Baldwin J W 2006 Effect of viscous loss on mechanical resonators designed for mass detection *Appl. Phys. Lett.* **88** 041921.
[27] Landau L and Lifshitz E 1966 *Fluid Mechanics* Pergamon Press Ltd., London.